

# Peierls distortion as a route to high thermoelectric performance in $\text{In}_4\text{Se}_{3-\delta}$ crystals

Jong-Soo Rhye<sup>1</sup>, Kyu Hyoung Lee<sup>1</sup>, Sang Mock Lee<sup>1</sup>, Eunseog Cho<sup>1</sup>, Sang Il Kim<sup>1</sup>, Eunsung Lee<sup>1</sup>, Yong Seung Kwon<sup>2</sup>, Ji Hoon Shim<sup>3</sup> & Gabriel Kotliar<sup>4</sup>

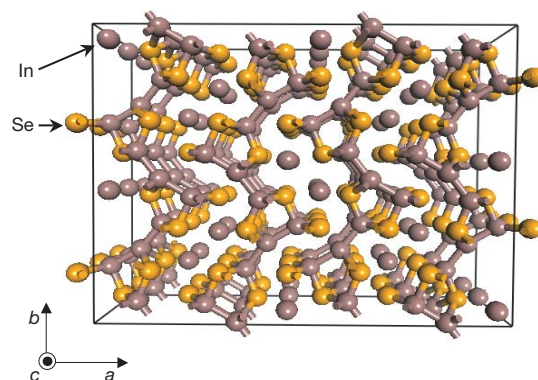
Thermoelectric energy harvesting—the transformation of waste heat into useful electricity—is of great interest for energy sustainability. The main obstacle is the low thermoelectric efficiency of materials for converting heat to electricity, quantified by the thermoelectric figure of merit,  $ZT$ . The best available n-type materials for use in mid-temperature (500–900 K) thermoelectric generators have a relatively low  $ZT$  of 1 or less, and so there is much interest in finding avenues for increasing this figure of merit<sup>1</sup>. Here we report a binary crystalline n-type material,  $\text{In}_4\text{Se}_{3-\delta}$ , which achieves the  $ZT$  value of 1.48 at 705 K—very high for a bulk material. Using high-resolution transmission electron microscopy, electron diffraction, and first-principles calculations, we demonstrate that this material supports a charge density wave instability which is responsible for the large anisotropy observed in the electric and thermal transport. The high  $ZT$  value is the result of the high Seebeck coefficient and the low thermal conductivity in the plane of the charge density wave. Our results suggest a new direction in the search for high-performance thermoelectric materials, exploiting intrinsic nanostructural bulk properties induced by charge density waves.

Over the past decade, there has been a renewed focused effort on thermoelectric materials motivated by the increasing societal needs for renewable energy and by technological advances in nanoscale science. The thermoelectric performance of a given material is characterized by the materials' dimensionless figure of merit  $ZT$  ( $ZT = S^2\sigma T/\kappa$ , where  $Z$ ,  $S$ ,  $\sigma$ ,  $T$ , and  $\kappa$  are respectively a measure of the material's thermoelectric properties, Seebeck coefficient, electrical conductivity, absolute temperature, and thermal conductivity), which can be enhanced by following two approaches. The first seeks to minimize the thermal conductivity by promoting phonon scattering and localization while preserving the itineracy of the electron transport<sup>2–6</sup>. The second seeks to enhance the power factor  $S^2\sigma$  through the quantum confinement effect in reduced dimensionalities<sup>7,8</sup>.

Recently, a new approach to ultralow thermal conductivity was explored. It was suggested that the layered structure of disordered two-dimensional crystalline sheets may have extremely low thermal conductivity<sup>9</sup>. Based on this, we propose the possible application of charge density waves (CDWs) to thermoelectricity. The CDW is a low-dimensional transport phenomenon involving strong electron–phonon coupling<sup>10</sup>. This strong interaction breaks the translational symmetry of lattices. The in-plane lattice distortion by CDWs of layered structured materials may realize the concept of layered and disordered crystalline sheets. In spite of the possible low thermal conductivity in a CDW system, it is necessary to select one type of carrier transport (electron or hole) to achieve a high power factor, because mixed carrier transport (electrons and holes) suppresses the Seebeck coefficient<sup>11</sup>.  $\text{In}_4\text{Se}_3$  provides an interesting realization of a material

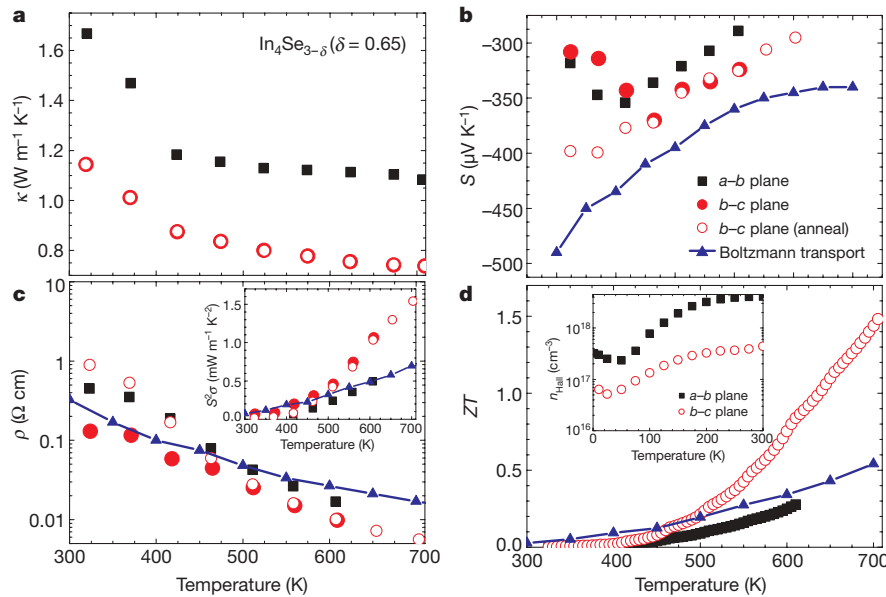
with reduced dimensionality, supporting quasi-one-dimensional In-chains<sup>12</sup>, nanorod structures<sup>13</sup>, and asymmetric band dispersion<sup>14</sup>. The crystal structure of  $\text{In}_4\text{Se}_3$  is shown in Fig. 1. It forms a layered structure of  $(\text{In}_3)^{5+}$  clusters covalently bonded to Se ions in the  $b$ – $c$  planes held together by van der Waals interactions along the  $a$  axis. Although the layered crystal structure is similar to the conventional  $\text{Bi}_2\text{Te}_3$  compound, the intrinsic properties of the nanorod structure and the quasi-one-dimensional chains of  $\text{In}_4\text{Se}_3$  are different from those of  $\text{Bi}_2\text{Te}_3$  and similar alloyed compounds. It is a bandgap semiconductor having a sizable bandgap of 0.5–1.0 eV with anisotropic band dispersions<sup>14</sup>. To reduce the energy of the bandgap, we employed self doping by Se deficiency, that is, a compound of formula  $\text{In}_4\text{Se}_{3-\delta}$ . We successfully grew two Se-deficient  $\text{In}_4\text{Se}_{3-\delta}$  crystal ingots;  $\text{In}_{59}\text{Se}_{41}$  ( $\text{In}_4\text{Se}_{2.78}$ ,  $\delta = 0.22$ ) and  $\text{In}_{63}\text{Se}_{37}$  ( $\text{In}_4\text{Se}_{2.35}$ ,  $\delta = 0.65$ ). From X-ray diffraction of the cross-sectional plane of the grown crystal, we find that the growth direction contains the  $a$ – $b$  plane, whereas the perpendicular to the growth direction has two mixed crystalline orientations of  $b$ – $c$  and  $a$ – $c$  planes (Supplementary Information); here we denote the perpendicular to the growth direction as the  $b$ – $c$  plane, for convenience, because electrical conduction is thought to be dominant along the  $b$ – $c$  plane, based on the results of band structure calculation of  $\text{In}_4\text{Se}_{3-\delta}$  ( $\delta = 0.25$ ).

Figure 2 shows representative thermoelectric properties of  $\text{In}_4\text{Se}_{2.35}$  ( $\delta = 0.65$ ) along the growth direction ( $a$ – $b$  plane, squares) and perpendicular to the growth direction ( $b$ – $c$  plane, red circles), together with results from theoretical Boltzmann transport calculations. As shown in Fig. 2a, the thermal conductivity  $\kappa(T)$  of  $\text{In}_4\text{Se}_{2.35}$  is very low ( $\leq 1.2 \text{ W m}^{-1} \text{ K}^{-1}$  at 300 K) along the  $b$ – $c$  plane, and it



**Figure 1 | Crystal structure of  $\text{In}_4\text{Se}_3$ .** Perspective view of the  $a$ – $b$  plane. Covalently bonded In–Se layers are stacked along the  $a$ -axis direction by relatively strong van der Waals interactions.

<sup>1</sup>Materials Research Laboratory, Samsung Advanced Institute of Technology, Yongin 446-712, Korea. <sup>2</sup>Department of Physics, Sung Kyun Kwan University, Suwon 440-746, Korea. <sup>3</sup>Department of Chemistry, Pohang University of Science and Technology, Pohang 790-784, Korea. <sup>4</sup>Department of Physics and Astronomy, Rutgers University, Piscataway, New Jersey 08854-8019, USA.



**Figure 2 | Anisotropic thermoelectric properties, annealing effect, and angle-averaged value of Boltzmann transport calculations for  $\text{In}_4\text{Se}_{3-\delta}$  ( $\delta = 0.65$ ) bulk crystal.** Shown are thermoelectric properties along the  $a$ - $b$  (squares) and  $b$ - $c$  planes (circles). Symbols shown both open and filled indicate measurements before and after heat treatment (450 °C, 24 h),

decreases with increasing temperature ( $0.74 \text{ W m}^{-1} \text{ K}^{-1}$  at 705 K). The thermal conductivities before and after heat treatment (450 °C for 24 h) are almost identical along the  $b$ - $c$  plane (open red circles).

The Seebeck coefficient  $S(T)$  and electrical resistivity  $\rho(T)$  are presented in Fig. 2b and 2c, respectively. Compounds of formula  $\text{In}_4\text{Se}_{3-\delta}$  ( $\delta \leq 0.65$ ) are n-type materials with negative Seebeck coefficient. Before heat treatment,  $\text{In}_4\text{Se}_{3-\delta}$  ( $\delta = 0.65$ ) exhibits a sharp dip in  $S$  near 415 K ( $a$ - $b$  plane) and 465 K ( $b$ - $c$  plane) which is close to the bulk melting temperature of the excess indium ( $T_m \approx 430 \text{ K}$ ). The low temperature thermal instability can be eliminated by annealing the sample at 450 °C for 24 h, which gives reproducible data without the transitions, as shown in Fig. 2b (red open circles). The electrical resistivity  $\rho(T)$  before and after heat treatment shows semiconducting behaviour of  $\rho(T)$  (Fig. 2c). Although the low-temperature values of  $S(T)$  and  $\rho(T)$  are affected by the excess In, the annealing effect is not significant in the regime which is relevant for thermoelectricity at temperatures higher than  $T_m$ .

The dimensionless figure of merit  $ZT$  shown in Fig. 2d reaches the remarkably high value of 1.48 for  $\text{In}_4\text{Se}_{2.35}$  ( $\delta = 0.65$ ) at 705 K along the  $b$ - $c$  plane. In the case of  $\text{In}_4\text{Se}_{2.78}$  ( $\delta = 0.22$ ),  $ZT$  reaches 1.1 at the same temperature (Supplementary Information). The higher  $ZT$  values of  $\text{In}_4\text{Se}_{2.35}$  ( $\delta = 0.65$ ) than those of  $\text{In}_4\text{Se}_{2.78}$  ( $\delta = 0.22$ ) are mainly caused by the lowering of thermal conductivity with increasing Se deficiency owing to the defect-induced phonon scattering at the Se-defect sites. The energy recycling efficiency  $\eta$  is calculated from the relation<sup>1</sup>;

$$\eta = \frac{\Delta T}{T_h} \frac{\sqrt{1+ZT} - 1}{\sqrt{1+ZT} + \frac{T_c}{T_h}}$$

where  $T_h$  ( $T_c$ ) is the hot(cold)-side temperature and  $\Delta T/T_h$  is the Carnot efficiency. The efficiency  $\eta$  for waste heat recovery of  $\text{In}_4\text{Se}_{2.35}$  ( $\delta = 0.65$ ) can reach 11.4% when  $T_h$  is 705 K and the temperature difference  $\Delta T = 300 \text{ K}$ . It could generate commercially viable levels of power by recycling waste heat in this mid-temperature range. The Hall carrier concentration  $n_{\text{Hall}}$  of the  $\text{In}_4\text{Se}_{2.35}$  ( $\delta = 0.65$ ) crystal for crystal orientations along the  $a$ - $b$  and the  $b$ - $c$  planes, determined by Hall resistivity measurements, is estimated to be  $4 \times 10^{18} \text{ cm}^{-3}$  and  $4 \times 10^{17} \text{ cm}^{-3}$  at 300 K, respectively (Fig. 2d inset). The carrier concentrations for the  $\text{In}_4\text{Se}_{3-\delta}$  compounds of  $\delta = 0.22$  and  $\delta = 0.65$

respectively. Blue triangles and lines indicate the result of the Boltzmann transport calculations. **a**, Temperature-dependent thermal conductivities,  $\kappa(T)$ . **b**, Seebeck coefficient,  $S(T)$ . **c**, Electrical resistivity,  $\rho(T)$ , and power factor defined by  $S^2\sigma$  (inset). **d**, Dimensionless figure-of-merit  $ZT$  and effective carrier concentration,  $n_{\text{eff}}$  (inset).

( $7 \times 10^{18} \text{ cm}^{-3}$  along the  $a$ - $b$  plane for  $\delta = 0.22$ ) are lower than the optimum carrier concentration ( $10^{19}$ – $10^{20} \text{ cm}^{-3}$ ) for narrow bandgap semiconductors<sup>15</sup>.

To understand the microscopic origin of the exceptional properties of this material, we performed first-principles transport calculations of  $\text{In}_4\text{Se}_3$  using the BoltzTraP program<sup>16</sup>. Calculations of the angle-averaged transport coefficients, within the rigid band approximation, can account for the experimental trends and confirm the potential of  $\text{In}_4\text{Se}_{3-\delta}$  as a thermoelectric material. Using a chemical potential  $\mu = 0.22 \text{ eV}$  and a scattering time  $\tau = 2.2 \times 10^{-14} \text{ s}$ , we obtained an electron concentration of  $1 \times 10^{18} \text{ cm}^{-3}$  and a high Seebeck coefficient ( $-360 \mu\text{V K}^{-1}$  at 600 K), which is comparable to the observed experimental value. The calculated temperature-dependent behaviour of  $S(T)$  and  $\rho(T)$  can qualitatively reproduce the experimental data, as shown in Fig. 2b and 2c (blue line and blue triangles). Using a constant value of the angle-averaged lattice thermal conductivity  $\kappa_{\text{ph}} = 0.8 \text{ W m}^{-1} \text{ K}^{-1}$ , we can account for the temperature dependence of the power factor and  $ZT$ , as shown in the inset of Fig. 2c and Fig. 2d, respectively. Within the rigid band approximation, the carrier density of those compounds is not yet optimal (Supplementary Information), and therefore  $ZT$  could be further increased by optimizing the carrier concentration by means of chemical substitutions.

High-resolution transmission electron microscopy (HRTEM) images and electron diffraction patterns are presented in Fig. 3. Figure 3a shows the HRTEM image of the  $a$ - $b$  plane of the  $\text{In}_4\text{Se}_{2.78}$  ( $\delta = 0.22$ ) crystal. The Bragg spots of the electron diffraction pattern in the  $a$ - $b$  plane (Fig. 3a inset) accompany small superstructure peaks in the chain direction. Quasi-one-dimensional Bragg spots and secondary superstructure peaks indicate the lattice distortion along the chain direction. Figure 3b shows the HRTEM image of the cross-sectional plane of the  $\text{In}_4\text{Se}_{2.78}$  ( $\delta = 0.22$ ) crystal ingot. There are several grain boundaries between the stripe and checkerboard patterns with arbitrary orientation: the stripe and checkerboard patterns are considered to be the  $a$ - $c$  and  $b$ - $c$  planes, respectively. The grains are about 20 nm or less in width. The electron diffraction pattern of the  $b$ - $c$  plane shows a rhomboidal Bragg diffraction pattern with one-dimensional superlattice peaks between the bright Bragg peaks (Fig. 3b inset), indicating the presence of a Peierls instability along the  $b$ -axis direction.

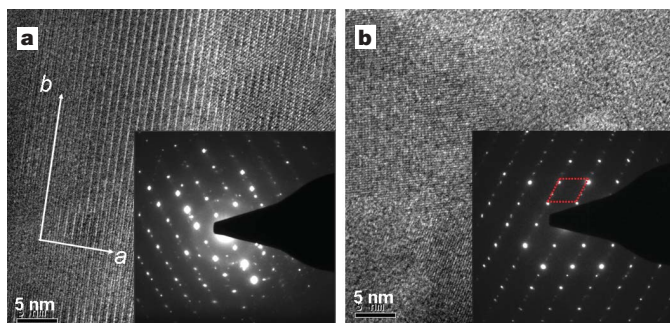


**Figure 3 | High-resolution TEM images and electron diffraction patterns of  $\text{In}_4\text{Se}_{3-\delta}$  ( $\delta = 0.22$ ).** **a**, HRTEM image of the  $a$ - $b$  plane. The one-dimensional chains are periodically aligned along the  $b$  direction. Inset, the electron diffraction pattern in the  $a$ - $b$  plane. The diffraction patterns of the quasi-one-dimensional chains are revealed along the  $b$  direction. Bragg spots with superstructure peaks along the  $b$  direction are due to the commensurate lattice distortions. **b**, HRTEM image of the cross-sectional plane of the grown crystal. Arbitrarily aligned chequerboard and stripe phases are of  $b$ - $c$  and  $a$ - $c$  planes. Inset, electron diffraction pattern of the  $b$ - $c$  plane. Red rhomboid indicates the diffraction pattern of unit cell.

The Peierls instability of this material is also suggested by theoretical considerations, once we explicitly include the Se vacancies in the calculations. We calculated the generalized electron susceptibility  $\chi(q)$ , where  $q$  is the momentum vector (ref. 17), from the band structure of  $\text{In}_4\text{Se}_{3-\delta}$  ( $\delta = 0.25$ );  $\chi(q)$  is shown along the  $X$ - $U$  symmetry line in Fig. 4b. The sharp peak at the  $(0, 1/2, 1/16)$  point can be understood from the quasi-one-dimensional Fermi surface nesting in the  $b$ - $c$  plane shown in Fig. 4a. It consists of two smooth diamond-shaped Fermi surfaces located at the upper and lower zone boundaries of the first Brillouin zone. There is a well defined commensurate nesting vector  $\mathbf{q}$  (red arrow) defined in the  $b$ - $c$  plane which can result in a CDW instability once the electron-phonon or electron-electron correlations are incorporated in a calculation going beyond the local-density approximation. Because of the long range lattice modulation along the  $c$  direction, the density wave instability is closely connected to the quasi-one-dimensional Peierls instability of the chain-like structure along the  $b$  axis of this material.

The electron diffraction pattern shown in Fig. 3b inset is consistent with this Fermi surface nesting behaviour. The small faint peaks between the Bragg spots indicate the doubling superstructure in the  $b$  direction, while the long-range modulation in the  $c$  direction cannot be seen, probably owing to the experimental resolution. Lattice distortion along the  $b$  axis is clearly visible in the electron diffraction pattern shown in Fig. 3a inset.

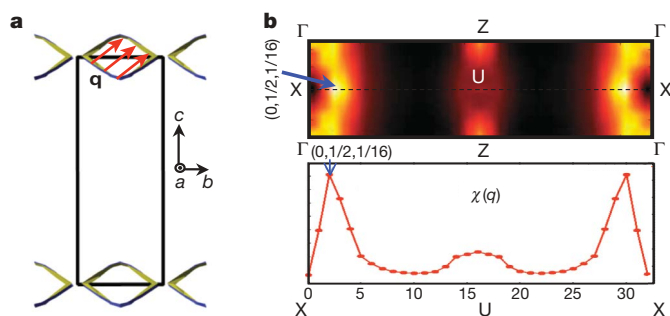


**Figure 4 | Fermi surface and generalized electron susceptibility of  $\text{In}_4\text{Se}_{3-\delta}$ .** **a**, Fermi surface of  $\text{In}_4\text{Se}_{3-\delta}$  ( $\delta = 0.25$ ) in the  $b$ - $c$  plane (blue and green lines). Black square is the first Brillouin zone. Fermi nesting vector  $\mathbf{q}$  (red arrow) is defined in the closed Fermi surface. **b**, Generalized electron susceptibility  $\chi(q)$  along the  $X(0, 1/2, 0)$ - $U(0, 1/2, 1/2)$  symmetry line (top). The  $\chi(q)$  has a singularity at the  $(0, 1/2, 1/16)$  point (bottom). The numbers on the horizontal axis indicates the calculation mesh along the  $X$ - $U$ - $X$  symmetry line.

Thermal transport properties shown in Fig. 2 also suggest the presence of a CDW. We note that the thermal conductivity in the  $b$ - $c$  plane is lower than that in the  $a$ - $b$  plane in the  $\text{In}_4\text{Se}_{2.35}$  crystal, which is at first sight surprising, as the bonding in the  $b$ - $c$  plane is weaker than in the  $a$ - $b$  plane. The in-plane ( $b$ - $c$  plane) lattice distortion driven by the CDW lowers the thermal conductivity. In addition, the Hall carrier concentration is anisotropic with respect to crystal orientations. In usual cases, the carrier density is isotropic with respect to crystal orientations. However, in this case, the carrier density along the  $b$ - $c$  plane is lower than that of the  $a$ - $b$  plane, which is caused by the CDW along the  $b$ - $c$  plane. Because of the CDW gap opening, the itinerant carrier density is decreased along the  $b$ - $c$  plane. These facts, and the  $S(T)$  and  $\rho(T)$  shown in Fig. 2b and c, suggest the formation of a CDW at a temperature higher than 705 K.

The theoretical calculations in the rigid band approximation of the  $\text{In}_4\text{Se}_{3-\delta}$  compound cannot however account for the observed anisotropy of the transport coefficients (see Supplementary Information for details). The rigid band approximation does not take into account the CDW with supercell zone boundaries. The quasi-one-dimensional lattice distortion, and the exotic anisotropic properties of thermal and electrical transport coefficients, together indicate the important role of the CDW in achieving a high  $ZT$  in the  $b$ - $c$  plane. The in-plane lattice distortion by CDW lowers thermal conductivity, and the intrinsic nanostructural low dimensionality of this material results in the high Seebeck coefficient.

The present thermoelectric investigations of  $\text{In}_4\text{Se}_{3-\delta}$  crystals suggest that bulk low-dimensional layered materials with strong electron-phonon coupling, such as Peierls or CDW instabilities, are promising candidates for new thermoelectric materials. Compared to other realizations of high- $ZT$  n-type thermoelectric materials through nanoscale phase separation<sup>18,19</sup>, the CDW mechanism for high  $ZT$  has the advantage of being realized as an intrinsically bulk phenomenon without artificial control of nanoscale phase segregation. This resulted in an exceptionally high  $ZT$  (1.48 at 705 K) in compounds with high chemical stability and good mechanical properties that can be combined with well established p-type thermoelectrics (such as skutterudites) to produce highly efficient thermoelectric power generation modules.

## METHODS SUMMARY

The  $\text{In}_4\text{Se}_{3-\delta}$  crystal ingots were grown by the Bridgeman method. In and Se were placed in an evacuated quartz ampoule with an excess of In (5–10 at.%) for Se-deficiency control. Heat treatment was followed by the melting and crystallizing at 550 °C and 590 °C for  $\delta = 0.65$  and 0.22 compounds, respectively, during a week with a growth rate of 1.5 mm h<sup>-1</sup>. The chemical inhomogeneity was examined by inductively coupled plasma spectroscopy and electron dispersive spectroscopy measurements. High-temperature thermal conductivity was obtained by measurements of sample density  $\rho_s$ , thermal diffusivity  $\lambda$  (by the laser flash method), and heat capacity  $C_p$  (in an ULVAC system);  $\kappa = \rho\lambda C_p$ , where heat capacity  $C_p$  was derived from Dulong-Petit fitting at high temperatures ( $T \geq 300$  K). The high-temperature electrical resistivity and Seebeck coefficient were measured by the four-probe method (in an ULVAC system). The Hall resistivity  $\rho_{xy}$  measurement was carried out by the five-contact AC-transport technique, using a physical property measurement system (Quantum Design). The effective carrier concentration was calculated by the one-band model as the following relation:  $n_{\text{eff}} = -1/(R_{\text{H}}e)$ , where the Hall coefficient  $R_{\text{H}} = \rho_{xy}/H$  and  $e = 1.602 \times 10^{-19}$  C.

The first-principles calculation was performed by the pseudopotential plane wave method using the Vienna *Ab initio* Simulation Package. We adopted the generalized gradient approximation implemented by Perdew, Burke, and Ernzerhof for the exchange correlation energy functional with the spin-orbit interaction. The thermoelectric properties are calculated using the BoltzTraP program.

Received 22 January; accepted 20 April 2009.

1. Snyder, G. J. & Toberer, E. S. Complex thermoelectric materials. *Nature Mater.* 7, 105–114 (2008).
2. Sales, B. C. Electron crystals and phonon glasses: a new path to improved thermoelectric materials. *Mater. Res. Soc. Bull.* 23, 15–21 (1998).

- Snyder, G. J., Christensen, M., Nishibori, E. J., Caillat, T. & Iversen, B. B. Disordered zinc in  $\text{Zn}_4\text{Sb}_3$  with phonon-glass and electron-crystal thermoelectric properties. *Nature Mater.* **3**, 458–463 (2004).
- Wölfing, B., Kloc, C., Teubner, J. & Bucher, E. High performance thermoelectric  $\text{Tl}_9\text{BiTe}_6$  with an extremely low thermal conductivity. *Phys. Rev. Lett.* **86**, 4350–4353 (2001).
- Boukai, A. I. *et al.* Silicon nanowires as efficient thermoelectric materials. *Nature* **451**, 168–171 (2007).
- Venkatasubramanian, R., Siivola, E., Colpitts, T. & O'Quinn, B. Thin-film thermoelectric devices with high room-temperature figures of merit. *Nature* **413**, 597–602 (2001).
- Dresselhaus, M. S. *et al.* New directions for low-dimensional thermoelectric materials. *Adv. Mater.* **19**, 1043–1053 (2007).
- Lin, Y.-M. & Dresselhaus, M. S. Thermoelectric properties of superlattice nanowires. *Phys. Rev. B* **68**, 075304 (2003).
- Chiritescu, C. *et al.* Ultralow thermal conductivity in disordered, layered  $\text{WSe}_2$  crystals. *Science* **315**, 351–353 (2007).
- Güner, G. *Density Waves in Solids* (Addison-Wesley, 1994).
- Rhyee, J. S. *et al.* Thermal and electronic transport properties of  $\text{CeTe}_{2-x}\text{Sn}_x$  compounds. *J. Appl. Phys.* **105**, 053712 (2009).
- Losovyj, Y. B. *et al.* The electronic structure of surface chains in the layered semiconductor  $\text{In}_4\text{Se}_3$  (100). *Appl. Phys. Lett.* **92**, 122107 (2008).
- Balitskii, O. A., Savchyn, V. P., Jaeckel, B. & Jaegermann, W. Surface characterization of  $\text{In}_4\text{Se}_3$  single crystals. *Physica E* **22**, 921–923 (2004).
- Losovyj, Y. B. *et al.* The anisotropic band structure of layered  $\text{In}_4\text{Se}_3$  (001). *J. Appl. Phys.* **104**, 083713 (2008).
- Mahan, G., Sales, B. & Sharp, J. Thermoelectric materials: new approaches to an old problem. *Phys. Today* **50**, 42–47 (March 1997).
- Madsen, G. K. H. & Singh, D. J. BoltzTraP. A code for calculating band-structure dependent quantities. *Comput. Phys. Commun.* **175**, 67–71 (2006).
- Shim, J. H., Kang, J.-S. & Min, B. I. Electronic structures of  $\text{RTE}_2$  ( $R=\text{La, Ce}$ ): a clue to the pressure-induced superconductivity in  $\text{CeTe}_{1.82}$ . *Phys. Rev. Lett.* **93**, 156406 (2004).
- Hsu, K. F. *et al.* Cubic  $\text{AgPb}_m\text{SbTe}_{2+m}$ : bulk thermoelectric materials with high figure of merit. *Science* **303**, 818–821 (2004).
- Chen, N. *et al.* Macroscopic thermoelectric inhomogeneities in  $(\text{AgSbTe}_2)_x(\text{PbTe})_{1-x}$ . *Appl. Phys. Lett.* **87**, 171903 (2005).

**Supplementary Information** is linked to the online version of the paper at [www.nature.com/nature](http://www.nature.com/nature).

**Acknowledgements** We thank D. Johnson, K. Koumoto and B. I. Min for discussions. We also thank H. R. Choi for TEM measurements. J.H.S. was supported by the WCU programme (KOSEF: R32-2008-000-10180-0).

**Author Information** Reprints and permissions information is available at [www.nature.com/reprints](http://www.nature.com/reprints). Correspondence and requests for materials should be addressed to S.M.L. ([sangmocklee@samsung.com](mailto:sangmocklee@samsung.com)).